Bloch-Floquet waves in flexural systems with continuous and discrete elements

Giorgio Carta[a], Michele Brun[a,*]

[a]*Dipartimento di Ingegneria Meccanica, Chimica e dei Materiali, Università di Cagliari, Piazza d'Armi, 09123 Cagliari, Italy*

Abstract

In this paper we describe the dynamic behavior of elongated multi-structured media excited by flexural harmonic waves. We examine periodic structures consisting of continuous beams and discrete resonators disposed in various arrangements. The transfer matrix approach and Bloch-Floquet conditions are implemented for the determination of different propagation and non-propagation regimes. The effects of the disposition of the elements in the unit cell and of the contrast in the physical properties of the different phases have been analyzed in detail, using representations in different spaces and selecting a proper set of non-dimensional parameters that fully characterize the structure. Coupling in series and in parallel continuous beam elements and discrete resonators, we have proposed a class of micro-structured mechanical systems capable to control wave propagation within elastic structures.

Keywords:
flexural waves, bi-coupled structures, transfer matrix, Bloch-Floquet conditions, dispersion properties, propagation zones

1. Introduction

Waves propagating in a homogeneous continuum are non-dispersive, since their phase and group velocities coincide. Conversely, in a structured medium (e.g. a rod, a beam or a plate) dispersion occurs due to the presence of

*Corresponding author
Email addresses: giorgio_carta@unica.it (Giorgio Carta), mbrun@unica.it (Michele Brun)

physical boundaries. A heterogeneous medium is also characterized by stop-bands, which are intervals of frequencies at which waves decay exponentially. Heterogeneities may be represented either by an intrinsic microstructure or by structural interfaces.

Some real structures are made of modular units, equal to each other, that are joined together. Despite being finite in reality, these structures can be analyzed as infinite sequences of identical elements connected to each other ("periodic structures"), as demonstrated by Wei and Petyt (1997a,b) for beams, by Brun et al. (2011) for bridges and by Carta et al. (2014a,b) for damaged strips.

Wave propagation in periodic structures has been extensively studied. In his classical treatise Brillouin (1953) gave a unified formulation for different classes of problems. In the literature, periodic structures are labeled according to the order of the equation describing the motion of the structure. It is usually convenient to express a differential equation of order p as a system of p first-order differential equations as, for example, in Stroh (1962), Lekhnitskii (1963) and Ting (1996). The number of kinematic independent variables $(p/2)$ defines the coupling at the interface between two modular units (or "unit cells"): "mono-coupled" if $p/2 = 1$, "bi-coupled" if $p/2 = 2$, and so on (see Mead (1975a,b)). Mono-coupled periodic structures (such as rods, one-dimensional lattices, etc.) were investigated by Mead (1975a), Faulkner and Hong (1985) and, more recently, by Martinsson and Movchan (2002), Brun et al. (2010), Carta and Brun (2012). Bi-coupled periodic structures (like beams) were examined by Mead (1975b, 1996), Heckl (2002), Romeo and Luongo (2002) and Carta et al. (2014a,b). In this paper, attention is focused on bi-coupled periodic structures, with particular interest to civil engineering structures (bridges, pipelines, railways, etc.), micro-mechanical systems (e.g. periodic MEMS bridges) and biological systems (like neurons).

The study of linear problems in elastodynamics has been carried out with different approaches. Heckl (2002), Movchan and Slepyan (2007), Brun et al. (2011), Movchan and Slepyan (2014) implemented a quasi-periodic Green's function, complemented in Movchan et al. (2007) and McPhedran et al. (2009) by the multipole expansion method for defects of finite size. A more direct procedure consists in solving directly the equations of motion by introducing the proper boundary conditions, as in Bigoni and Movchan (2002), Gei et al. (2009) and Brun et al. (2013). The transfer matrix method (Pestel and Leckie (1963), Faulkner and Hong (1985), Lekner (1994), Castanier and Pierre (1995), Romeo and Luongo (2002), Brun et al. (2010))

proves to be an efficient tool for increasingly complex periodic structures, in the sense that complicated unit cells can be easily decomposed into simpler sub-units while the dimension of the transfer matrix is independent of the complexity of the unit cell. In this work we will use the transfer matrix approach for continuous and discrete bi-coupled systems connected in series and in parallel.

The determination of the dispersion properties of the system and of pass- and stop-bands (i.e. the intervals of frequencies in which waves can propagate or not) can be performed in different ways. The most common approach is to use the dispersion relation, which shows the dependence of the frequency on the wavenumber or wavevector. The analysis of the invariants of the transfer matrix is useful to determine all possible propagation characteristics of a periodic structure. The identification of propagation and non-propagation zones in a physical-space, where the coordinate variables are the physical parameters of the structure, is of primary importance for the design of filtering systems. Another approach is based on the study of the eigenvalues of the characteristic (or secular) equation of the periodic structure. These four alternative techniques are outlined in Section 2 (the reader may also refer to the extensive analysis by Romeo and Luongo (2002) for a more detailed discussion of the mentioned techniques). Section 3 presents the study of wave propagation in four types of bi-coupled periodic structures, consisting of different arrangements of continuous and discrete elements (or "phases") connected either in series or in parallel. The periodic systems described in Section 3 are employed in different engineering structures. For instance, beams in parallel connected at regular distances (Section 3.2) are used to design bridges (Fig. 1a), warehouses or other buildings. Also composite beams made of concrete slabs and steel girders with shear connectors (Fig. 1b) can be framed in the context of parallel beams. Brun et al. (2013a,b) proposed a new design of bridges, which is based on the introduction of a by-pass system, which redirects waves propagating within the structure and annihilates the motion of the main deck of the bridge. On the other hand, discrete oscillators (Sections 3.3 and 3.4) are inserted into a structure to mitigate its vibrations in a narrow range of frequencies. Examples of discrete oscillators include viscous dampers (Fig. 1c) and tuned mass dampers (Fig. 1d). We note that viscosity is not taken into account in the study of Sections 3.3 and 3.4. Systems with multiple tuned mass dampers are studied by Zuo and Nayfeh (2005).

We point out that a finite-thickness interface can produce filtering, fo-

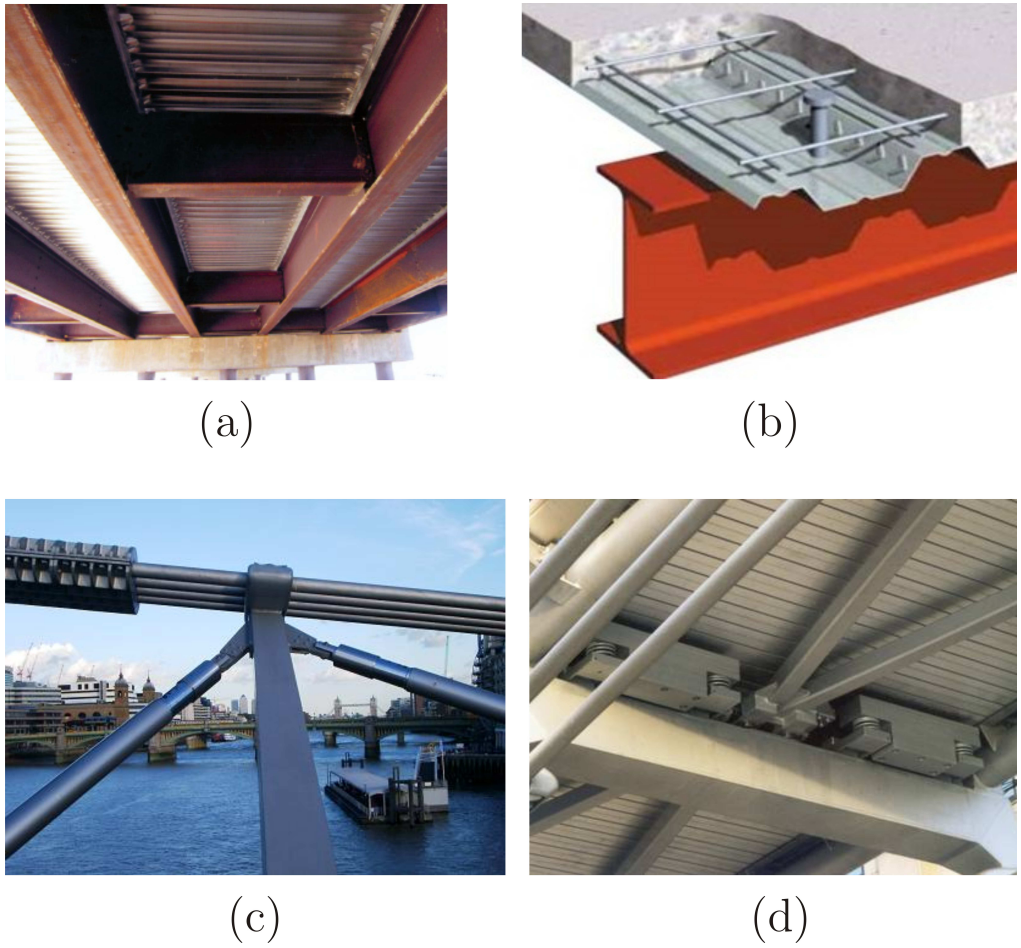

Figure 1: (a) Steel girders of a bridge crossing Box Elder Creek in Watkins, Colorado, USA (from www.shortspansteelbridges.org, accessed on 08/09/2014); (b) detail of a composite beam consisting of a concrete slab, steel girders and shear connectors (from www.theconstructor.org, accessed on 08/09/2014); (c) viscous dampers used in the Millennium Bridge, London, UK (from www.mace.manchester.ac.uk, accessed on 09/09/2014); (d) tuned mass dampers employed in the Millennium Bridge, London, UK (from www.gerbusa.com, accessed on 09/09/2014).

cussing and localization effects on the continuous media connected by it, as firstly shown by Bigoni and Movchan (2002). Brun et al. (2010) used the concept of structural interface to design a metamaterial for elastic waves that leads to negative refraction phenomena. In view of the above considerations, the analytical results of this paper can be exploited to design special devices

that work as flexural wave filters or vibration absorbers.

2. Dispersion properties of bi-coupled systems

We consider flexural harmonic waves propagating within periodic systems made of Euler-Bernoulli beams. These bi-coupled periodic structures will be hereafter referred to as "periodic beams".

The equation of motion for the transverse displacement $v(x)$ of an Euler-Bernoulli beam is

$$EJv^{IV} - \rho A\omega^2 v = 0, \tag{1}$$

where E is the Young's modulus, J the second moment of inertia, ρ the mass density, A the cross-sectional area and ω the angular frequency.

2.1. Transfer Matrix

The vectors of generalized displacements and forces at the end and at the beginning of the n^{th} unit cell, located respectively at $x = x_{n+1}$ and $x = x_n$, are connected by the transfer matrix $\boldsymbol{M}$ through the following relation:

$$\boldsymbol{U}_{n+1} = \begin{Bmatrix} v(x_{n+1}) \\ \theta(x_{n+1}) \\ M(x_{n+1}) \\ T(x_{n+1}) \end{Bmatrix} = \boldsymbol{M}\,\boldsymbol{U}_n = \boldsymbol{M} \begin{Bmatrix} v(x_n) \\ \theta(x_n) \\ M(x_n) \\ T(x_n) \end{Bmatrix}, \tag{2}$$

where v, $\theta = v'$, $M = -EJv''$ and $T = -EJv'''$ represent vertical displacement, rotation, bending moment and shear force, respectively, while EJ is the flexural stiffness of the beam. We emphasize that the transfer matrix $\boldsymbol{M}$ depends on the angular frequency ω and that it can be defined to relate generalized displacements and forces at any two different positions such as, for example, the boundaries of a sub-unit of the unit cell.

With reference to the unit cell, Bloch-Floquet conditions require that the following equation be satisfied:

$$\det\left[\boldsymbol{M} - e^{\mathrm{i}kL}\,\boldsymbol{I}\right] = 0. \tag{3}$$

Here $\boldsymbol{I}$ is the 4x4 identity matrix, k denotes the wavenumber (or, equivalently, the Bloch-Floquet parameter) and $L = x_{n+1} - x_n$ is the length of the unit cell. Eq. (3) represents the dispersion relation of the periodic beam, since it provides the dependence of the angular frequency ω on the wavenumber

k. The dispersion relation allows to distinguish the frequencies of the waves that propagate without attenuation ("pass-bands") from the frequencies of the waves that decay exponentially ("stop-bands"). More specifically, pass-bands and stop-bands are obtained when the wavenumber assumes real and imaginary values, respectively. The dispersion relation gives also information on the phase and group velocities of the propagating waves (see Brillouin (1960)).

2.2. Invariant properties

Alternatively, the identification of the pass- and stop-bands can be carried out by evaluating the eigenvalues or the invariants of the transfer matrix, as suggested by Romeo and Luongo (2002). The characteristic equation of the periodic beam is given by

$$\det\left[\boldsymbol{M}-\lambda\,\boldsymbol{I}\right]=0 \quad \Rightarrow \quad \lambda^4-I_1\lambda^3+I_2\lambda^2-I_3\lambda+I_4=0, \tag{4}$$

where $I_1, I_2, I_3, I_4 \in \mathbb{R}$ represent the invariants of $\boldsymbol{M}$, while the four solutions λ_i $(i = 1, 2, 3, 4)$ of Eq. (4) are the eigenvalues of $\boldsymbol{M}$. Since $\boldsymbol{M}$ is a symplectic matrix, the eigenvalues have the 'reciprocal property', namely if λ_i is a solution also its reciprocal $(\lambda_j = 1/\lambda_i)$ is a solution (see Yao et al. (2009)). Furthermore, the coefficients of Eq. (4) are symmetric and have the following expressions:

$$I_3 = I_1 = \mathrm{tr}\left(\boldsymbol{M}\right), \tag{5a}$$

$$I_2 = \frac{1}{2}\left[\mathrm{tr}^2\left(\boldsymbol{M}\right)-\mathrm{tr}\left(\boldsymbol{M}^2\right)\right], \tag{5b}$$

$$I_4 = \det\left(\boldsymbol{M}\right) = 1. \tag{5c}$$

In the formulae above, $\mathrm{tr}(\boldsymbol{M})$ and $\det(\boldsymbol{M})$ indicate the trace and the determinant of the transfer matrix $\boldsymbol{M}$, respectively.

2.2.1. Eigenvalues

If $|\lambda_i| = 1$ the corresponding wave propagates with constant amplitude, while if $|\lambda_i| < 1$ (> 1) the corresponding wave decays exponentially in the positive (negative) direction. Actually, for the reciprocal property mentioned above, only two eigenvalues need to be considered to fully characterize the propagation features of the periodic beam. This can be explained on physical grounds by considering that there are two waves traveling in the positive (forward) direction and two waves traveling in the negative (backward) direction, which have the same propagation properties.

2.2.2. Invariant space

The above considerations allow to distinguish the following zones in the invariant space $I_1 - I_2$: the *pass-pass* (PP) zones, where both waves propagate without attenuation; the *pass-stop* (PS) zones, where one wave decays exponentially and the other one propagates with constant amplitude; the *stop-stop* (SS) zones, where both waves decay exponentially; and the *complex* (C) zones, that are special SS zones in which the eigenvalues are complex conjugate and their moduli are different from 1. The invariant plane can be divided into seven zones, as shown in Fig. 2. The straight lines r and s and the parabola p plotted in Fig. 2, which represent the transitions between different propagation regimes, have the following expressions:

$$\mathrm{r} : I_2 = 2I_1 - 2, \tag{6a}$$

$$\mathrm{s} : I_2 = -2I_1 - 2, \tag{6b}$$

$$\mathrm{p} : I_2 = \frac{1}{4} I_1^2 + 2. \tag{6c}$$

In Fig. 2 and in the following figures, PP, PS and SS zones are colored in black, grey and white, respectively, while the dotted regions indicate the C zones.

The representation in Fig. 2 is valid for any periodic bi-coupled structure, even for expressions of bending moment and shear force more general than the ones specified after Eq. (2). When a specific structural system is considered, the dispersion curve is a path in the invariant space $I_1 - I_2$ parametrized by the frequency ω. For non-supported systems, as the ones considered in this paper, this path starts at the point $(I_1, I_2) = (4, 6)$, intersection point of the four zones. Then, it can lie in a single region (to the best of our knowledge this is the PS region) or cross different zones exhibiting band-gaps. For a homogeneous Euler-Bernoulli beam we can express the equation of motion (1) in the form

$$\nabla^4 v - \beta^4 v = (\nabla^2 + \beta^2)(\nabla^2 - \beta^2) v = 0, \tag{7}$$

where $\beta^4 = \omega^2 \, \rho A/(EJ)$ (β has the physical dimension of $[\mathrm{m}^{-1}]$). The solution of equation (7) admits the representation

$$v(x) = v_H(x) + v_M(x), \tag{8}$$

where

$$(\nabla^2 + \beta^2) v_H(x) = 0, \quad (\nabla^2 - \beta^2) v_M(x) = 0. \tag{9}$$

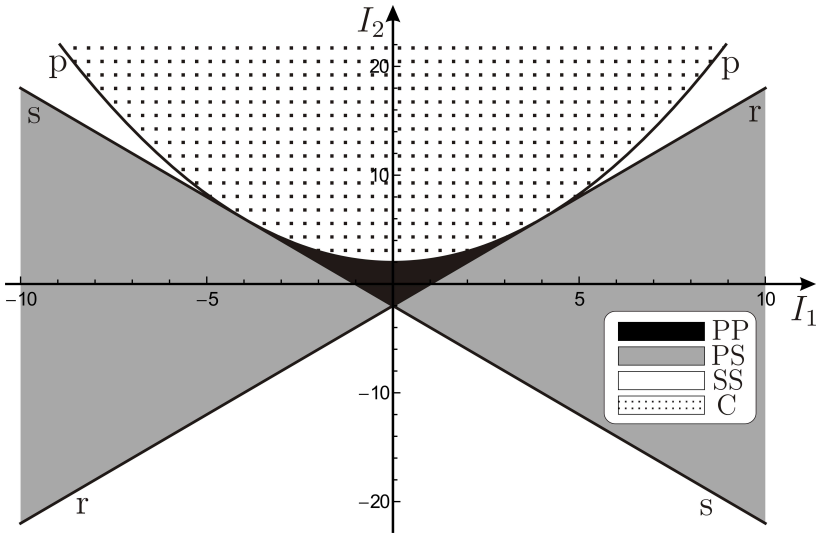

Figure 2: Propagation zones in the invariant space $I_1 - I_2$ (see also Romeo and Luongo (2002)). Pass-pass (PP), pass-stop (PS), stop-stop (SS) and complex (C) regions are shown in different colors.

Thus v is the superposition of propagating waves of Helmholtz type v_H and non-propagating waves of modified Helmholtz type v_M, corresponding to PS regions. Conversely, for an Euler-Bernoulli beam on an elastic foundation, the path starts in the C region and enters the PS region crossing the point $(I_1, I_2) = (4, 6)$ at the cut-off frequency $\omega = \sqrt{\gamma/(\rho A)}$, γ being the foundation stiffness.

The representation in the invariant space allows to identify directly propagation and non-propagation regions of the structure, but it does not give information on the transition frequencies and on the wavenumber. In particular, it is useful to detect the cases in which the system allows to enter the PP zone, which is located between PS and C regions. In Section 3.2 we will show and discuss in detail such an uncommon case, in which two different waves propagate in both directions.

2.3. Physical space

An alternative way is to describe the dispersion properties in the physical space, introducing a set of physical parameters that characterize the periodic system. Such representation is particularly convenient for design purposes, in the sense that it shows directly the effect of the geometrical, constitutive and

inertial parameters on the transmission properties of the elastic structure. To represent the propagation zones in a plane, it is necessary to fix all the physical parameters except two, one of which is the non-dimensional frequency. To build the representation in the physical space it is convenient to express the invariants in terms of the physical parameters and substitute the new expressions of the invariants into Eqs. (6), which thus define the boundaries between different propagation zones in the physical space. We note that the mapping between the invariant and physical spaces is non-linear.

3. Continuous and discrete systems in series and parallel

In this section we analyze dispersion properties of flexural periodic systems. In particular, we consider continuous beams coupled with translational and rotational oscillators. We will show how the topology of the unit cell can lead to innovative filtering properties.

3.1. Continuous phases in series

We first consider the case of two continuous beams arranged in series and rigidly connected to each other. A schematic representation of this periodic system is shown in Fig. 3, where the lengths of the two phases are indicated by l_1 and l_2, while E_i, J_i, ρ_i and A_i ($i = 1, 2$) denote the Young's modulus, the second moment of inertia, the mass per unit volume and the cross-sectional area of each phase i, respectively.

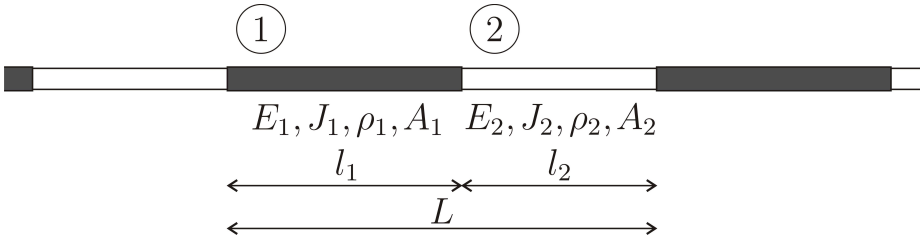

Figure 3: Periodic beam consisting of two continuous phases in series with rigid connections.

The construction of the transfer matrix $\boldsymbol{M}_i$ of each phase i is discussed in Appendix A and the expression is given by Eq. (A.6).

The transfer matrix $\boldsymbol{M}^{[I]}$ of the periodic beam sketched in Fig. 3 results to be

$$\boldsymbol{M}^{[I]} = \boldsymbol{M}_2 \, \boldsymbol{M}_1. \tag{10}$$

In the above and following equations, the numbers in square brackets distinguish among the different examples of periodic beams considered in this paper. The expression (10) is obtained imposing continuity conditions for all the components of the generalized vector at the boundaries between the two phases.

Four non-dimensional parameters are needed to completely describe this periodic model. We define the *impedance ratio*, the *natural frequency ratio*, the *length ratio* and the *frequency parameter* as

$$\xi = \sqrt{\frac{Q_1}{Q_2}} = \sqrt[4]{\frac{E_1 J_1 \rho_1 A_1}{E_2 J_2 \rho_2 A_2}} = \sqrt{\frac{\beta_1^2 E_1 J_1}{\beta_2^2 E_2 J_2}}, \tag{11a}$$

$$\eta = \frac{\omega_1}{\omega_2} = \sqrt{\frac{E_1 J_1 \rho_2 A_2}{E_2 J_2 \rho_1 A_1}} \frac{l_2^2}{l_1^2}, \tag{11b}$$

$$\lambda = \frac{l_1}{l_2}, \tag{11c}$$

$$\Omega = \sqrt{\frac{\omega}{\overline{\omega}}}, \tag{11d}$$

respectively. Here $Q_i = \sqrt{E_i J_i \rho_i A_i}$ and $\omega_i = \sqrt{E_i J_i/(\rho_i A_i)}/l_i^2$ stand for the impedance and the natural frequency of each phase i, respectively, while $\beta_i = (\rho_i A_i \omega^2/(E_i J_i))^{1/4}$. The low-frequency homogenized natural frequency of the cell $\overline{\omega}$ is obtained from the homogenized flexural stiffness $\overline{EJ}$ (harmonic average) and the homogenized linear density $\overline{\rho A}$ (geometric average) as follows

$$\overline{\omega} = \sqrt{\frac{\overline{EJ}}{\overline{\rho A}}} \frac{1}{L^2} = \sqrt{\frac{\left[\frac{1}{L}\left(\frac{l_1}{E_1 J_1} + \frac{l_2}{E_2 J_2}\right)\right]^{-1}}{\frac{\rho_1 A_1 l_1 + \rho_2 A_2 l_2}{L}}} \frac{1}{L^2}. \tag{12}$$

Here the term 'low-frequency homogenized natural frequency' is used to indicate the range of frequencies and wavenumbers where the relation between $\sqrt{\omega}$ and k is approximately linear. The invariants of the transfer matrix $\boldsymbol{M}^{[I]}$

can be evaluated as functions of the four parameters given by Eqs. (11):

$$
\begin{aligned}
I_1^{[I]} = \frac{1}{8}\Bigg\{ & \left(\xi + \frac{1}{\xi}\right)^2 \Bigg[\left(\frac{1}{\sqrt{\lambda\sqrt{\eta}}} + \sqrt{\lambda\sqrt{\eta}} \right)^2 \left(\cos\left(\phi_1+\phi_2\right) + \cosh\left(\phi_1+\phi_2\right)\right) \\
& \qquad - \left(\frac{1}{\sqrt{\lambda\sqrt{\eta}}} - \sqrt{\lambda\sqrt{\eta}} \right)^2 \left(\cos\left(\phi_1-\phi_2\right) + \cosh\left(\phi_1-\phi_2\right)\right) \Bigg] \\
& + \mathrm{i}\left(\xi - \frac{1}{\xi}\right)^2 \Bigg[\left(\frac{1}{\sqrt{\lambda\sqrt{\eta}}} + \mathrm{i}\sqrt{\lambda\sqrt{\eta}} \right)^2 \left(\cos\left(\phi_1+\mathrm{i}\phi_2\right) + \cosh\left(\phi_1+\mathrm{i}\phi_2\right)\right) \\
& \qquad - \left(\frac{1}{\sqrt{\lambda\sqrt{\eta}}} - \mathrm{i}\sqrt{\lambda\sqrt{\eta}} \right)^2 \left(\cos\left(\phi_1-\mathrm{i}\phi_2\right) + \cosh\left(\phi_1-\mathrm{i}\phi_2\right)\right) \Bigg] \Bigg\},
\end{aligned}
\tag{13a}
$$

$$
\begin{aligned}
I_2^{[I]} = & \frac{1}{4}\left[2\lambda\sqrt{\eta} + \frac{1}{\lambda\sqrt{\eta}}\left(\xi^2 + \frac{1}{\xi^2}\right)\right] \left[\sinh\left(\left(1+\mathrm{i}\right)\phi_1\right) + \sin\left(\left(1+\mathrm{i}\right)\phi_1\right)\right] \\
& \times \left[\sinh\left(\left(1+\mathrm{i}\right)\phi_2\right) - \sin\left(\left(1+\mathrm{i}\right)\phi_2\right)\right] + \frac{1}{4}\left[\frac{2}{\lambda\sqrt{\eta}} + \lambda\sqrt{\eta}\left(\xi^2 + \frac{1}{\xi^2}\right)\right] \\
& \times \left[\sinh\left(\left(1+\mathrm{i}\right)\phi_1\right) - \sin\left(\left(1+\mathrm{i}\right)\phi_1\right)\right] \left[\sinh\left(\left(1+\mathrm{i}\right)\phi_2\right) + \sin\left(\left(1+\mathrm{i}\right)\phi_2\right)\right] \\
& - \left(\lambda^2\eta + \frac{1}{\lambda^2\eta} + \xi^2 + \frac{1}{\xi^2}\right) \sinh\left(\phi_1\right)\sin\left(\phi_1\right)\sinh\left(\phi_2\right)\sin\left(\phi_2\right) \\
& + \frac{1}{4}\left(\xi^4 + \frac{1}{\xi^4}\right)\left[1 - \cosh\left(\phi_1\right)\cos\left(\phi_1\right)\right]\left[1 - \cosh\left(\phi_2\right)\cos\left(\phi_2\right)\right] \\
& + \frac{1}{2}\left[3 + \cosh\left(\phi_1\right)\cos\left(\phi_1\right) + \cosh\left(\phi_2\right)\cos\left(\phi_2\right)\right. \\
& \left. + 7\cosh\left(\phi_1\right)\cos\left(\phi_1\right)\cosh\left(\phi_2\right)\cos\left(\phi_2\right)\right].
\end{aligned}
\tag{13b}
$$

In the formulae above, ϕ_1 and ϕ_2 are the two non-dimensional quantities

$$
\phi_1 = \beta_1 l_1 = \Omega \sqrt[4]{\frac{\lambda^2\xi^2}{\left(1+\lambda\right)^2\left(1+\lambda\eta\xi^2\right)\left(\xi^2+\lambda\eta\right)}} \tag{14a}
$$

and

$$
\phi_2 = \beta_2 l_2 = \Omega \sqrt[4]{\frac{\lambda^2\xi^2\eta^2}{\left(1+\lambda\right)^2\left(1+\lambda\eta\xi^2\right)\left(\xi^2+\lambda\eta\right)}} = \sqrt{\eta}\phi_1, \tag{14b}
$$

respectively.

Setting the *length ratio* $\lambda = 1/2$ and the *natural frequency ratio* $\eta = 1/\lambda^2 = 4$, Eqs. (13) assume the simplified expressions

$$
\begin{aligned}
I_1^{[I]} = & \frac{1}{2}\left(\xi + \frac{1}{\xi}\right)^2 \left[\cosh\left(3\phi\right) + \cos\left(3\phi\right)\right] - \frac{1}{4}\left(\xi - \frac{1}{\xi}\right)^2 \\
& \times \left[\cosh\left(\left(1+2\mathrm{i}\right)\phi\right) + \cos\left(\left(1+2\mathrm{i}\right)\phi\right) + \cosh\left(\left(2+\mathrm{i}\right)\phi\right) + \cos\left(\left(2+\mathrm{i}\right)\phi\right)\right],
\end{aligned}
\tag{15a}
$$

$$
\begin{aligned}
I_2^{[I]} = &\left(\xi+\frac{1}{\xi}\right)^2 \frac{\cosh(\phi)}{2}\left[\cosh\left((2+3\mathrm{i})\,\phi\right)+\cos\left((3+2\mathrm{i})\,\phi\right)-\cos(3\phi)-\cos(\phi)\right] \\
&+\frac{1}{4}\left(\xi^4+\frac{1}{\xi^4}\right)\left[1-\cosh(\phi)\cos(\phi)\right]\left[1-\cosh(2\phi)\cos(2\phi)\right] \\
&-\left(\xi+\frac{1}{\xi}\right)^2 \sinh(\phi)\sin(\phi)\sinh(2\phi)\sin(2\phi)+\frac{1}{2}\left[3+\cosh(\phi)\cos(\phi)\right. \\
&\left.+\cosh(2\phi)\cos(2\phi)+7\cosh(\phi)\cos(\phi)\cosh(2\phi)\cos(2\phi)\right],
\end{aligned}
\tag{15b}
$$

which are used for the numerical computations. The quantity ϕ appearing in Eqs. (15) is the non-dimensional frequency given by

$$
\phi = \phi_1 = \frac{\phi_2}{2} = \Omega \sqrt[4]{\frac{\xi^2}{9\left(1+2\xi^2\right)\left(2+\xi^2\right)}}. \tag{16}
$$

Dispersion curves are plotted in normalized coordinates in Fig. 4a, where curves correspond to *impedance ratios* $\xi = 1/4, 1/2, 1$. In Fig. 4b propagation zones are shown in the physical space $\phi - \xi$. The three cases shown in part (a) are represented by horizontal lines in the physical plane in part (b).

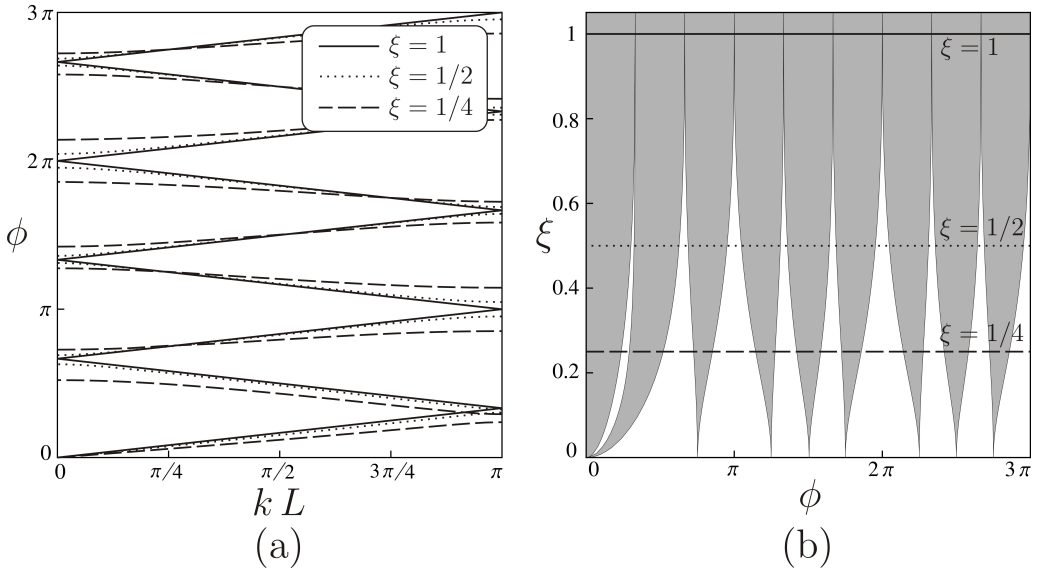

Figure 4: Dispersion curves (a) and physical plane $\phi - \xi$ representation (b) for a bi-phase continuous periodic beam. Curves are given for *natural frequency ratio* $\eta = 4$ and *length ratio* $\lambda = 1/2$. The cases with *impedance ratios* $\xi = 1/4, 1/2, 1$ are reported in part (b) as horizontal lines. PS regions are coloured in grey, while SS regions are indicated in white.

From Fig. 4a it is apparent that, if the beam is homogeneous ($\xi = 1$ and $\eta\lambda^2 = 1$), any frequency has an associated wave that propagates in the structure without attenuation, as predicted by the classical theory of wave motion in beams (see, for instance, Graff (1975), Ch. 3). The periodicity introduces an internal length and it causes the dispersion curve to be reflected at the boundary of the first Brillouin zone. Indeed, in the physical plane of Fig. 4b the solid line at $\xi = 1$ never crosses a stop-stop (SS) zone, but totally lies inside the pass-stop (PS) region. As the contrast between the impedances is increased by decreasing the value of ξ, stop-stop zones open up. It is clear from Fig. 4b that stop-bands are generated around frequencies that the dispersion curves of the homogeneous case $\xi = 1$ assume at $kL = 0$ and $kL = \pi$, except for the first stop-band which is located at lower frequencies as the *impedance ratio* decreases. It is also evident from Fig. 4a that the opening of stop-bands ($\xi \neq 1$) induces stationary waves at the boundaries of each propagation zone.

The paths in the invariant space $I_1 - I_2$ are shown in Figs. 5 for the three *impedance ratios* considered above. For the sake of clarity, the paths corresponding to increasing frequency intervals are shown from part (a) to part (d) of Fig. 5. As already shown in the representation in the physical space of Fig. 4b, only PS and SS regions can be obtained from this structured system. In particular, as the frequency increases, the paths - starting at point $(I_1, I_2) = (4, 6)$ and initially lying in the PS region - enter the SS regions alternatively from the boundary s at $kL = \pi$ and from the boundary r at $kL = 0$. The path corresponding to the homogeneous case always lies inside the PS region and it is tangent to the boundaries s and r at $kL = \pi$ and $kL = 0$, respectively.

It is interesting to analyze the conditions in a non-homogeneous system for which the path in the invariant space totally lies in the PS region, namely the conditions for which no stop-bands exist as in the homogeneous case. This event corresponds physically to the absence of reflections at the interfaces between the two phases. To this purpose, we look at the possibility to have the invariants in the same form as in the homogeneous case, i.e.

$$I_1 = 2\left[\cos(\hat{\phi}) + \cosh(\hat{\phi})\right] \quad \text{and} \quad I_2 = 2\left[1 + 2\cos(\hat{\phi})\cosh(\hat{\phi})\right], \tag{17}$$

where $\hat{\phi}$ is a generic angle to be found. Such form is obtained when

$$\xi = 1 \quad \text{and} \quad \lambda^2\eta = 1, \tag{18}$$

which imposes the requirement that the flexural stiffnesses and the linear densities of the two phases be the same:

$$E_1 J_1 = E_2 J_2 \quad \text{and} \quad \rho_1 A_1 = \rho_2 A_2. \tag{19}$$

Conditions (19) are much more restrictive than the requirement for mono-coupled systems, in which full propagation is assured if the two phases have the same impedance (see Brun et al. (2010)).

In Fig. 6 we plot the moduli of the two eigenvalues for each of the three values of ξ considered. As already mentioned in Section 2, a wave propagates without attenuation when the modulus of its eigenvalue is equal to 1, while it decays exponentially if it is different from 1. Fig. 6 shows that, in the present example, one wave always decays exponentially (grey lines), while the other one does or does not propagate depending on the frequency considered (black lines). The PS zones for each of the three cases analyzed are reproduced at the top of the figure and are, obviously, identical to those shown in Figs. 4.

Finally, we emphasize that different values of the *natural frequency ratio* η produce similar results.

3.2. Continuous phases in parallel

In this section we examine a periodic beam consisting of two continuous phases in parallel, which are connected at regular intervals of length L, as shown in Fig. 7. The connections prevent relative displacements and rotations between the two phases at the boundaries.

In order to derive the transfer matrix for this case, denoted as $\boldsymbol{M}^{[II]}$, the vectors of generalized displacements and forces at the left and right boundaries of each phase i ($i = 1, 2$) are partitioned as

$$\boldsymbol{U}_i(x) = \left\{ \begin{array}{c} \boldsymbol{W}_i(x) \\ \boldsymbol{F}_i(x) \end{array} \right\}, \tag{20}$$

with $x = x_l, x_r$ respectively. The vector $\boldsymbol{W}_i$ contains the kinematic components (vertical displacement and rotation), while the vector $\boldsymbol{F}_i$ includes the static components (bending moment and shear force). Accordingly, the transfer matrix $\boldsymbol{M}_i$ of each phase i is partitioned as

$$\boldsymbol{M}_i = \begin{bmatrix} \boldsymbol{M}_{i,11} & \boldsymbol{M}_{i,12} \\ \boldsymbol{M}_{i,21} & \boldsymbol{M}_{i,22} \end{bmatrix}. \tag{21}$$

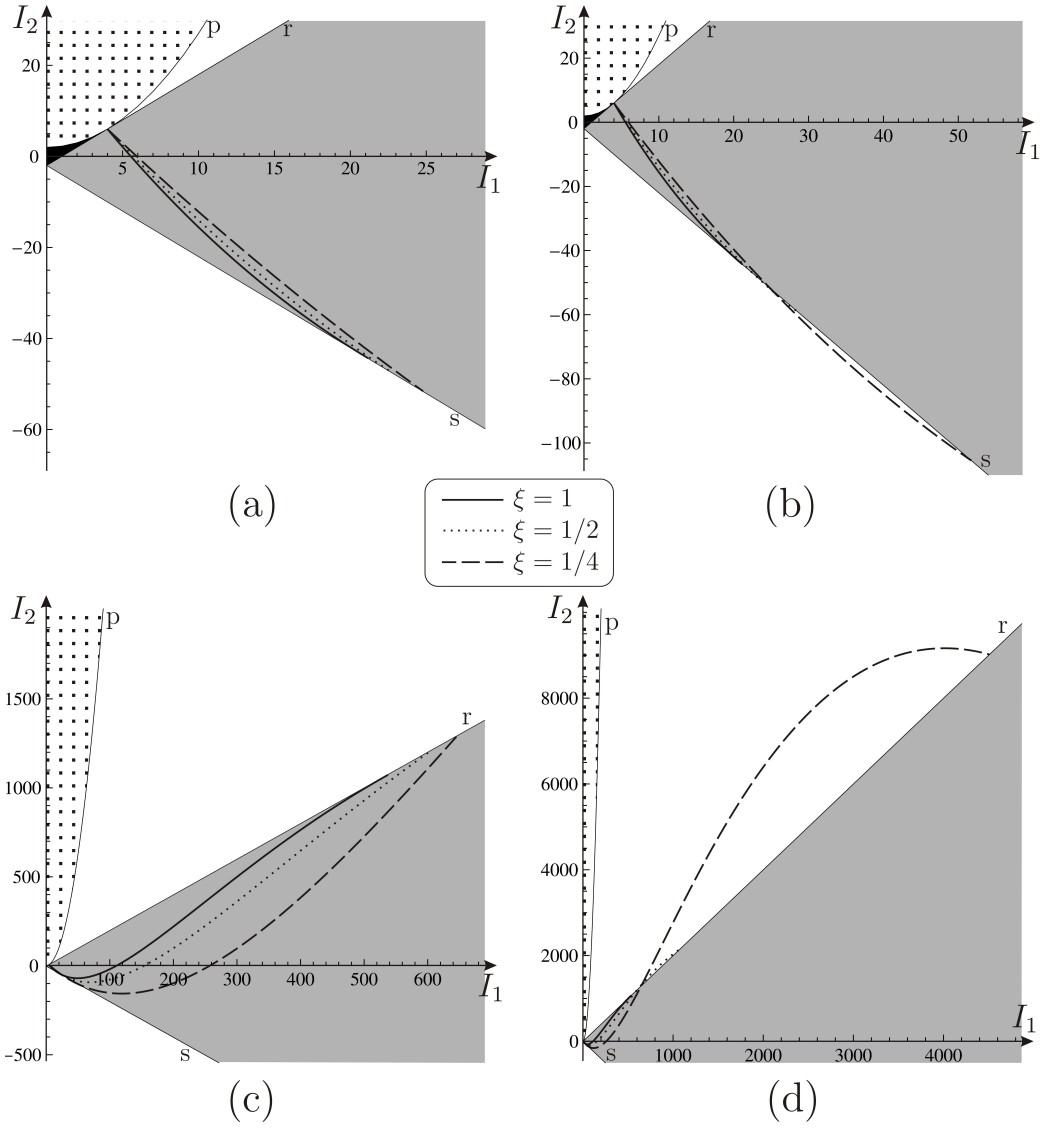

Figure 5: Representations in the invariant plane $I_1 - I_2$ for the periodic beam with two continuous phases in series. Three paths are given, corresponding to $\xi = 1/4, 1/2, 1$ and to $\eta = 4$ and $\lambda = 1/2$. Parts (a)-(d) correspond to increasing frequency intervals: at the beginning (a) and at the end (b) of the first stop-band ($kL = \pi$) and at the beginning (c) and at the end (d) of the second stop-band ($kL = 0$).

For bi-coupled periodic structures, each submatrix in Eq. (21) has dimensions 2x2. The compatibility conditions at the boundaries of the unit cell require

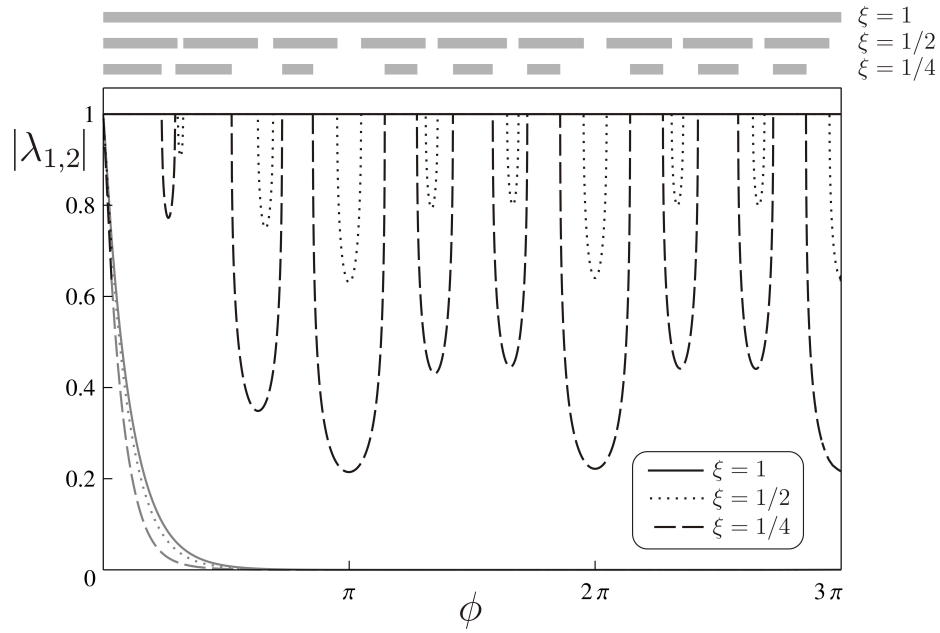

Figure 6: Dependence of the moduli of the two eigenvalues on the non-dimensional frequency ϕ for the periodic beam with two continuous phases in series (with $\xi = 1/4, 1/2, 1$, $\eta = 4$ and $\lambda = 1/2$).

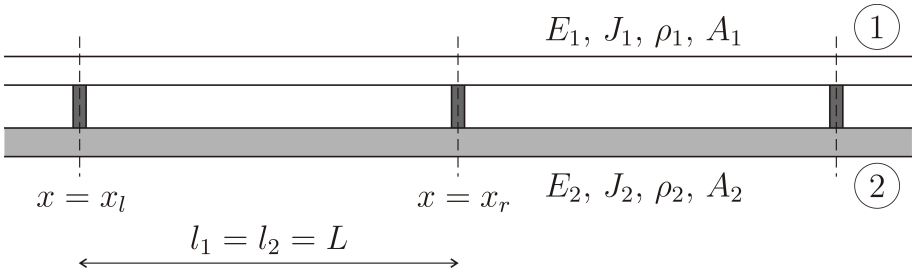

Figure 7: Periodic beam made of two continuous homogeneous beams in parallel, rigidly connected at regular distances L. Top view.

that

$$\boldsymbol{W}_1(x_l) = \boldsymbol{W}_2(x_l) = \boldsymbol{W}(x_l), \tag{22a}$$

$$\boldsymbol{W}_1(x_r) = \boldsymbol{W}_2(x_r) = \boldsymbol{W}(x_r), \tag{22b}$$

$$\boldsymbol{F}_1(x_l) + \boldsymbol{F}_2(x_l) = \boldsymbol{F}(x_l), \tag{22c}$$

$$\boldsymbol{F}_1(x_r) + \boldsymbol{F}_2(x_r) = \boldsymbol{F}(x_r), \tag{22d}$$

where $\boldsymbol{W}$ and $\boldsymbol{F}$ are the generalized vectors of kinematic and static variables of the unit cell. By using Eqs. (22), the transfer matrix $\boldsymbol{M}^{[II]}$ can be written in the following form:

$$\boldsymbol{M}^{[II]} = \begin{bmatrix} \boldsymbol{M}^{[II]}_{\alpha\alpha} & \boldsymbol{M}^{[II]}_{\alpha\beta} \\ \boldsymbol{M}^{[II]}_{\beta\alpha} & \boldsymbol{M}^{[II]}_{\beta\beta} \end{bmatrix}, \tag{23a}$$

with

$$\boldsymbol{M}^{[II]}_{\alpha\alpha} = \left(\boldsymbol{M}^{-1}_{1,12} + \boldsymbol{M}^{-1}_{2,12}\right)^{-1} \left(\boldsymbol{M}^{-1}_{1,12}\,\boldsymbol{M}_{1,11} + \boldsymbol{M}^{-1}_{2,12}\,\boldsymbol{M}_{2,11}\right), \tag{23b}$$

$$\boldsymbol{M}^{[II]}_{\alpha\beta} = \left(\boldsymbol{M}^{-1}_{1,12} + \boldsymbol{M}^{-1}_{2,12}\right)^{-1}, \tag{23c}$$

$$\begin{aligned} \boldsymbol{M}^{[II]}_{\beta\alpha} =& \boldsymbol{M}_{1,21} + \boldsymbol{M}_{2,21} - \boldsymbol{M}_{1,22}\,\boldsymbol{M}^{-1}_{1,12}\,\boldsymbol{M}_{1,11} - \boldsymbol{M}_{2,22}\,\boldsymbol{M}^{-1}_{2,12}\,\boldsymbol{M}_{2,11} \\ &+ \left(\boldsymbol{M}_{1,22}\,\boldsymbol{M}^{-1}_{1,12} + \boldsymbol{M}_{2,22}\,\boldsymbol{M}^{-1}_{2,12}\right) \left(\boldsymbol{M}^{-1}_{1,12} + \boldsymbol{M}^{-1}_{2,12}\right)^{-1} \\ &\times \left(\boldsymbol{M}^{-1}_{1,12}\,\boldsymbol{M}_{1,11} + \boldsymbol{M}^{-1}_{2,12}\,\boldsymbol{M}_{2,11}\right), \end{aligned} \tag{23d}$$

$$\boldsymbol{M}^{[II]}_{\beta\beta} = \left(\boldsymbol{M}_{1,22}\,\boldsymbol{M}^{-1}_{1,12} + \boldsymbol{M}_{2,22}\,\boldsymbol{M}^{-1}_{2,12}\right) \left(\boldsymbol{M}^{-1}_{1,12} + \boldsymbol{M}^{-1}_{2,12}\right)^{-1}. \tag{23e}$$

The expression of the transfer matrix given by Eqs. (23) can be applied to any structural system with continuous phases in parallel. For different couplings between the two beams, appropriate partitions of the generalized vector and transfer matrix have to be set.

We adopt the following physical parameters: *impedance ratio* ξ, *natural frequency ratio* η and *frequency parameter* Ω as in Eq. (11a), Eq. (11b) with $l_1 = l_2 = L$ and Eq. (11d), respectively. The homogenized flexural stiffness in Eq. (11d) is now $\overline{EJ} = E_1J_1 + E_2J_2$ and the *length ratio* $\lambda = 1$.

The dispersion curves are shown in Fig. 8 for the *natural frequency ratios* $\eta = 1, 10, 100$, while the propagation and non-propagation zones are illustrated in Fig. 9 in the physical planes Ω-η (part a) and ϕ-η (part b), where $\phi = \beta_2 L$.

When the two phases have the same natural frequency, so that $\eta = 1$, the invariants take the form (17) with $\hat{\phi} = \phi$, independently of the *impedance ratio* ξ, which is then taken equal to one. In other words, for $\eta = 1$ the system behaves as a homogeneous beam with natural frequency ϕ.

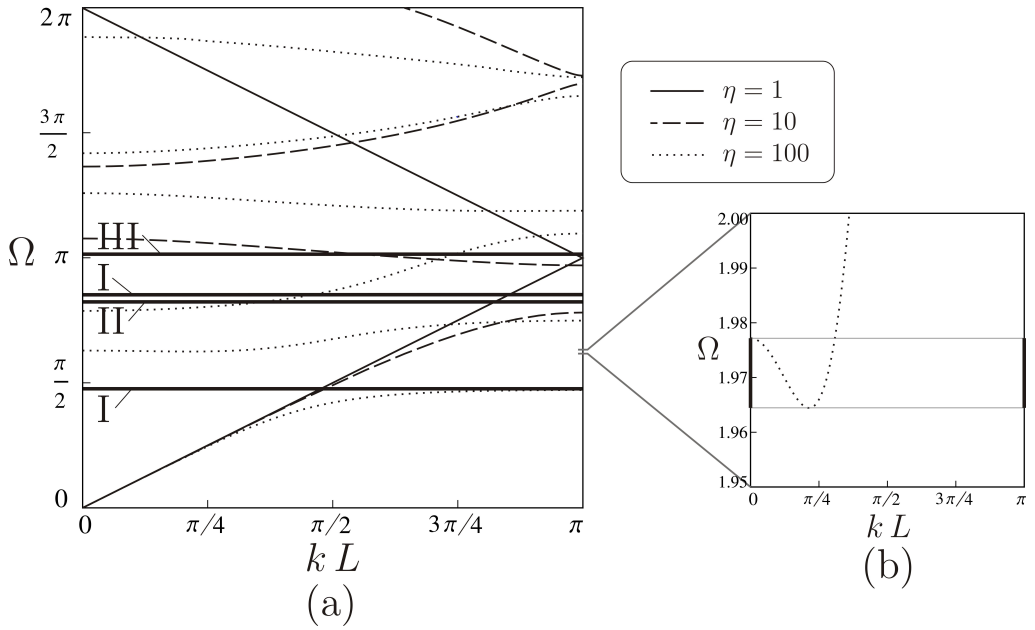

Figure 8: (a) Dispersion curves for the periodic beam depicted in Fig. 7. Results are given for *natural frequency ratios* $\eta = 1, 10, 100$ and *impedance ratio* $\xi = 1$. Lines I, II, III represent internal resonance modes. (b) Detail of (a) for the case $\eta = 100$, showing a range of frequencies characterized by two propagating waves with the same frequency and different wavenumbers, corresponding to a PP zone.

3.2.1. Pass-pass regions

As the contrast in the natural frequency increases, the dispersion curves drastically change and stop-bands do not open up at regular frequency intervals. From the representations in the physical spaces, it is evident that all the propagation regions, PS, SS, C and PP, can be reached, contrary to the case examined in Section 3.1 where the beams were connected in series.

In particular, the system allows to reach PP regions, as shown in Figs. 9; the zoom in Fig. 8b points out the possibility to have two propagating waves at the same frequency. Such property can find interesting applications in by-pass systems, as outlined in Brun et al. (2013a,b). PP regions can be obtained in few types of flexural systems. In a homogeneous Timoshenko beam, the motion of the system is described by the slope of the cross-section in addition to the transverse displacement. Thus there are two dispersion

equations, given by

$$\omega_{1,2} = \frac{G\hat{A}}{2\rho J}\left[1+\left(\frac{J}{A}+\frac{EJ}{G\hat{A}}\right)k^2 \pm \sqrt{1+\left(\frac{J}{A}-\frac{EJ}{G\hat{A}}\right)^2 k^4+2\left(\frac{J}{A}+\frac{EJ}{G\hat{A}}\right)k^2}\right], \quad (24)$$

where G is the shear modulus and $\hat{A}$ is the shear area (see Graff (1975)). Then, two waves coexist at frequencies $\omega \geq \omega_c = G\hat{A}/(\rho J)$. Nevertheless, when the system is sufficiently slender the value of ω_c is beyond the range of validity of the mono-dimensional beam model.

In presence of compressive prestress N and distributed elastic support of stiffness γ, the dispersion equation for the Euler-Bernoulli beam is

$$\omega = \sqrt{\frac{EJk^4 - Nk^2 + \gamma}{\rho A}} \quad (25)$$

and the system has two propagating waves in each direction in the interval $\sqrt{(4\gamma EJ - N^2)/(4\rho A\, EJ)} \leq \omega \leq \sqrt{\gamma/(\rho A)}$, as outlined in Carta (2012). Romeo and Luongo (2002) and Brun et al. (2011) have also shown the possibility to reach the PP region for a homogeneous Euler-Bernoulli beam on equally-spaced concentrated elastic supports for particular values of the support stiffness.

3.2.2. Internal resonance modes

In the dispersion diagrams of Fig. 8a some horizontal lines appear, indicated with the labels I, II and III. They correspond to the thick black lines in the physical spaces of Fig. 9. These lines represent extremely localized modes and correspond to singularities of the invariants I_1 and I_2, associated with eigenvalues moduli equal to zero. An example of internal resonance modes is reported in Fig. 10 for $\eta = 100$ and $\phi \simeq 4.732$ (line I). Fig. 10 shows that the energy is localized in one phase, the one having the lower natural frequency. For high natural frequency contrasts, it is possible to compute analytically the frequencies associated with such internal resonance modes. Indeed, for large values of η the invariants can be approximated as

$$I_1^{(2)} = 4 + \frac{F_1(\phi)}{\cos(\phi)\cosh(\phi) - 1}\,\frac{1}{\eta} + O\left(\frac{1}{\eta}\right)^{\frac{3}{2}}, \quad (26a)$$

$$I_2^{(2)} = 6 + \frac{F_2(\phi)}{\cos(\phi)\cosh(\phi) - 1}\,\frac{1}{\eta} + O\left(\frac{1}{\eta}\right)^{\frac{3}{2}}. \quad (26b)$$

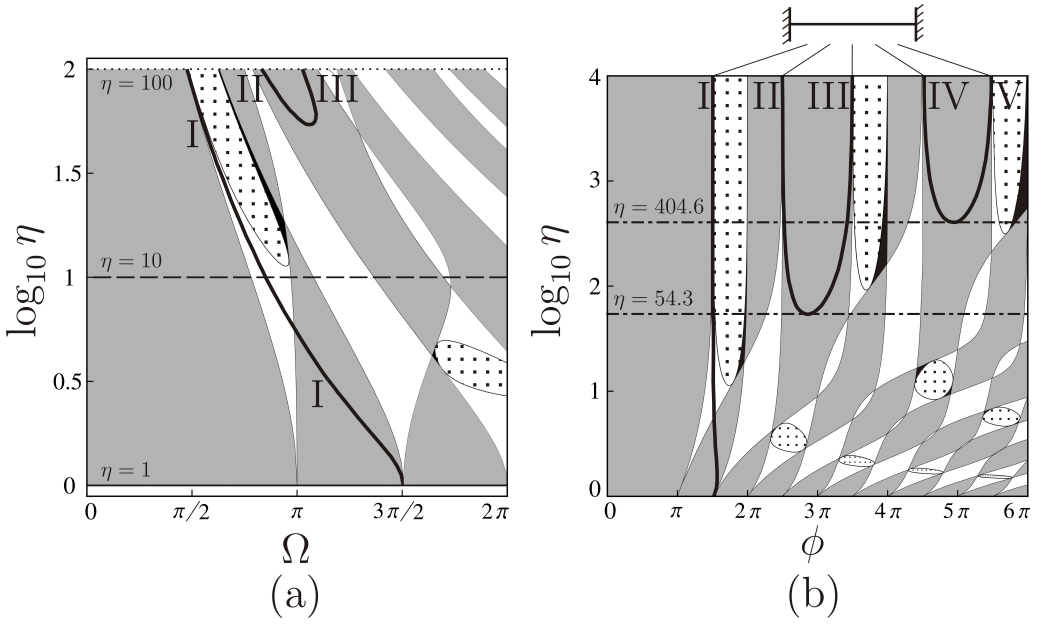

Figure 9: Propagation zones in the physical planes $\Omega - \eta$ (a) and $\phi - \eta$ (b), relative to the periodic beam of Fig. 7 with *impedance ratio* $\xi = 1$. In (a) the horizontal lines at $\eta = 1, 10, 100$ correspond to the dispersion curves in Fig. 8. Black thick lines I, II, III, IV, V represent internal resonance modes.

In the expressions above F_1 and F_2 are two bounded functions of ϕ, hence the invariants are singular when the denominator of the second coefficient of the expansion vanishes. The expression of the denominator coincides with the equation that provides the natural frequencies of a clamped-clamped homogeneous beam, indicated at the top of Fig. 9b.

We note that the number of internal resonance modes increases with η. The limiting values of η for which this number increases from one to three, $\eta = 54.3$, and from three to five, $\eta = 404.6$, are indicated in Fig. 9b.

Finally we point out that, in correspondence of these internal resonance modes, the propagation regions of the system do not change, as checked in the invariant space and from the study of the eigenvalues. Conversely, in mono-coupled systems similar resonance modes are associated with the opening of narrow stop-bands within pass-bands and opening of narrow pass-bands within stop-bands (see Brun and Sulis (in preparation)).

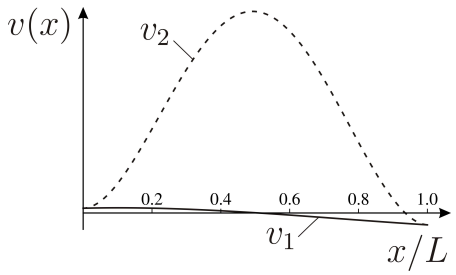

Figure 10: Eigenvector of a unit cell for $\xi = 1$, $\eta = 100$ and $\phi \simeq 4.732$, corresponding to line I in Figs. 8 and 9. v_1 and v_2 are the vertical displacements in beams 1 and 2, respectively, while L is the length of the unit cell.

3.3. Continuous phase and discrete masses in series

We consider a structured system made of continuous beam elements connected in series with discrete rotational and translational resonators, as shown in Fig. 11. The resonators have polar inertia and mass equal to J_{ms} and m_s, respectively, while k_{1s} and k_{2s} denote the translational and rotational equivalent stiffnesses of the springs joining the discrete masses to the continuous elements of the main structure.

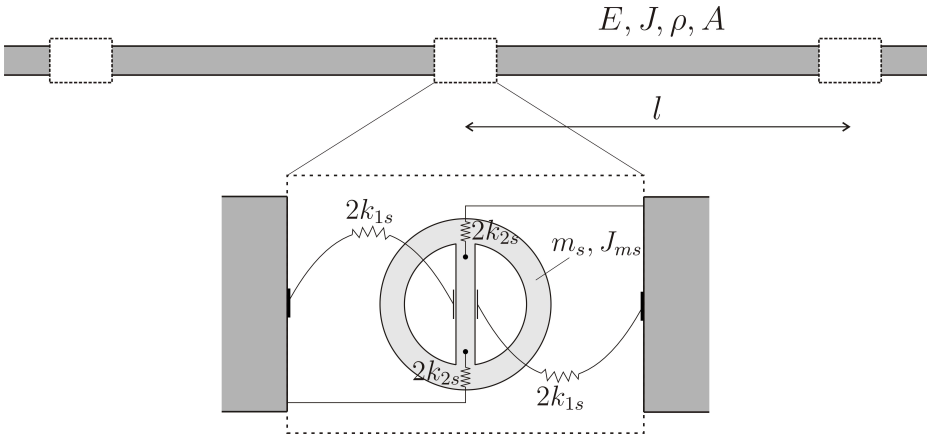

Figure 11: Periodic beam containing rotational and translational resonators connected in series to continuous beam elements.

The transfer matrix for the discrete system is constructed by imposing linear and angular momentum balance for the resonators. It takes the form

$\boldsymbol{I} + \boldsymbol{K_s}$, where

$$\boldsymbol{K_s} = \begin{bmatrix} -\frac{m_s\omega^2}{2k_{2s}} & 0 & 0 & \frac{1}{k_{2s}} - \frac{m_s\omega^2}{4k_{2s}^2} \\ 0 & -\frac{J_{ms}\omega^2}{2k_{1s}} & -\frac{1}{k_{1s}} + \frac{J_{ms}\omega^2}{4k_{1s}^2} & 0 \\ 0 & J_{ms}\omega^2 & -\frac{J_{ms}\omega^2}{2k_{1s}} & 0 \\ -m_s\omega^2 & 0 & 0 & -\frac{m_s\omega^2}{2k_{2s}} \end{bmatrix}. \tag{27}$$

Consequently, the transfer matrix for the unit cell is given by

$$\boldsymbol{M}^{[III]} = \boldsymbol{M}\ (\boldsymbol{I} + \boldsymbol{K_s}), \tag{28}$$

where $\boldsymbol{M}$, describing the homogeneous beam, is expressed by Eq. (A.6).

We define the non-dimensional *frequency parameter*, *inertial ratios* and *stiffness ratios* as

$$\Phi = \beta\, l = \sqrt[4]{\frac{\rho A\omega^2}{EJ}}\, l, \tag{29a}$$

$$M_s = \frac{J_{ms}}{\rho A l^3}, \quad \mu_s = \frac{m_s}{\rho A l}, \tag{29b}$$

$$\kappa_{1s} = \frac{k_{1s} l}{EJ}, \quad \kappa_{2s} = \frac{k_{2s} l^3}{EJ}. \tag{29c}$$

The invariants of $\boldsymbol{M}^{[III]}$ are expressed by

$$\begin{aligned} I_1^{[III]} = &\left[2 - \frac{\delta\Phi^4\,(1+\chi)}{2\chi\kappa_{2s}}\right]\,[\cos(\Phi) + \cosh(\Phi)] \\ &- \frac{\Phi}{2}\left[\delta\left(\Phi^2+1\right) + \frac{1}{\chi\kappa_{2s}}\left(\chi\Phi^2+1\right) - \frac{\delta\Phi^4}{4\chi^2\kappa_{2s}^2}\left(\chi^2\Phi^2+1\right)\right]\sin(\Phi) \\ &- \frac{\Phi}{2}\left[\delta\left(\Phi^2-1\right) + \frac{1}{\chi\kappa_{2s}}\left(\chi\Phi^2-1\right) - \frac{\delta\Phi^4}{4\chi^2\kappa_{2s}^2}\left(\chi^2\Phi^2-1\right)\right]\sinh(\Phi), \end{aligned} \tag{30a}$$

$$
\begin{aligned}
I_2^{[III]} = &\left[\frac{\delta^2\Phi^4}{2} + \frac{\delta^2\Phi^8}{8\chi\kappa_{2s}^2} + \left(\frac{1}{8\chi} + \frac{\Phi^4}{32\chi^2\kappa_{2s}^2}\right)\left(4 - \frac{\delta\Phi^4}{\kappa_{2s}}\right)\left(4\chi - \frac{\delta\Phi^4}{\kappa_{2s}}\right)\right] \\
&- \sin(\Phi)\Phi\left\{\left[\delta\left(\Phi^2+1\right) - \frac{\delta\Phi^4}{4\chi^2\kappa_{2s}^2}\left(1+2\chi+\chi\Phi^2\left(2+\chi\right)\right)\right.\right. \\
&\qquad \left. + \left(\chi\Phi^2+1\right)\left(\frac{1}{\chi\kappa_{2s}} - \frac{\delta^2\Phi^4}{2\chi\kappa_{2s}} + \frac{\delta^2\Phi^8}{8\chi^2\kappa_{2s}^3}\right)\right]\cosh(\Phi) \\
&\qquad \left. - \left[\frac{\delta\Phi}{\chi\kappa_{2s}}\left(\chi\Phi^4-1\right) - \frac{\delta^2\Phi^5}{4\chi^2\kappa_{2s}^2}\left(\chi^2\Phi^4-1\right)\right]\sinh(\Phi)\right\} \\
&- \cos(\Phi)\left\{\left[\frac{\delta^2\Phi^4}{2} + \frac{\Phi^4}{32\chi^2\kappa_{2s}^2}\left(4 - \frac{\delta\Phi^4}{\kappa_{2s}}\right)\left(4\chi - \frac{\delta\Phi^4}{\kappa_{2s}}\right) - 4\right.\right. \\
&\qquad \left. + \frac{3\delta\Phi^4}{2\chi\kappa_{2s}}\left(1+\chi\right) - \frac{3\delta^2\Phi^8}{4\chi\kappa_{2s}^2}\right]\cosh(\Phi) \\
&\qquad + \Phi\left[\delta\left(\Phi^2-1\right) + \frac{\delta\Phi^4}{4\chi^2\kappa_{2s}^2}\left(1+2\chi-\chi\Phi^2\left(2+\chi\right)\right)\right. \\
&\qquad \left.\left. + \left(\chi\Phi^2-1\right)\left(\frac{1}{\chi\kappa_{2s}} - \frac{\delta^2\Phi^4}{2\chi\kappa_{2s}} + \frac{\delta^2\Phi^8}{8\chi^2\kappa_{2s}^3}\right)\right]\sinh(\Phi)\right\},
\end{aligned}
\tag{30b}
$$

where we have set $M_s = \mu_s = \delta$ and $\chi = \kappa_{1s}/\kappa_{2s}$ is the *stiffness contrast*.

Dispersion curves are plotted in Figs. 12, while the representation in the physical plane $\Phi - \chi$ is shown in Figs. 13. Results are given for $\delta = 0.01$ and $\kappa_{2s} = 1$. Dispersion curves for $\chi = 0.1, 1, 10$ and for the homogeneous beam case are plotted in part (a) of Fig. 12, while in part (b) the case $\chi = 10^{-5}$ is presented.

The acoustic branch for the beam with oscillators is reduced in size with respect to the homogeneous case. At increasing frequencies pass-bands become narrower and narrower and they are positioned at regular frequency intervals, showing a transition from a continuous-like to a discrete-like behavior. Such property is also detected in mono-coupled systems (Brun et al. (2010), Brun and Sulis (in preparation)). The presence of very narrow pass-bands is due to the presence of discrete elements within the unit cell, which introduces a polynomial dependence on the *frequency parameter* Φ in the invariant expressions (30), while the position of the pass-bands is determined by the continuous phases. For $\chi \gg 1$, the central frequencies of the narrow pass-bands are $\Phi \simeq n\pi$ $(n = 3, 4, \ldots)$, corresponding to the natural frequencies of a double-guided simple beam having the same physical properties as the one composing the unit cell and shown at the top of Fig. 13a. In such a case, the high rotational stiffness does not allow rotations at the beam ends.

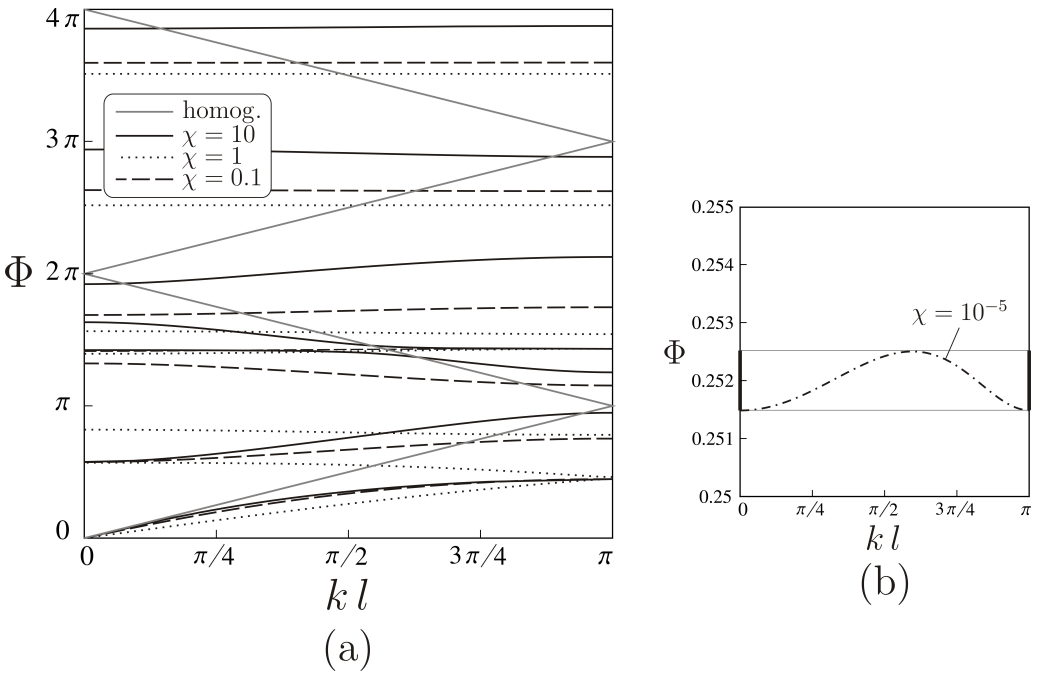

Figure 12: (a) Dispersion curves of the periodic beam shown in Fig. 11. Results are given for a continuous-discrete system with *stiffness contrasts* $\chi = 0.1, 1, 10$, *inertial ratios* $\delta = M_s = \mu_s = 0.01$ and *translational stiffness ratio* $\kappa_{2s} = 1$ and for a continuous homogeneous system corresponding to $\delta \to 0$, $\kappa_{1s}, \kappa_{2s} \to \infty$. (b) Detail of the dispersion diagram for the case $\chi = 10^{-5}$, showing a PP zone.

For $\chi \ll 1$, the central frequencies of the pass-bands are solutions of the characteristic equation $\cos(\Phi)\cosh(\Phi) = 1$ ($\Phi \simeq 10.996$, 14.137, 17.279, ...), which are the natural frequencies of a simple beam with free end rotations and vertical displacements, as shown at the bottom of Fig. 13a. In this case, the low rotational stiffness permits rotations at the beam ends.

Finally we notice that for the structured system analysed in this section all propagation zones are present, in particular the PP zone, as also demonstrated by the dispersion curve in Fig. 12b. In contrast with the case examined in Section 3.2, PP and C propagation zones are extremely small.

3.4. Continuous phase and discrete masses in parallel

Here we examine a case similar to that investigated in Section 3.3, but assuming that the oscillators are attached periodically to the continuous beam as in Fig. 14. In this application the polar inertia and the mass are referred

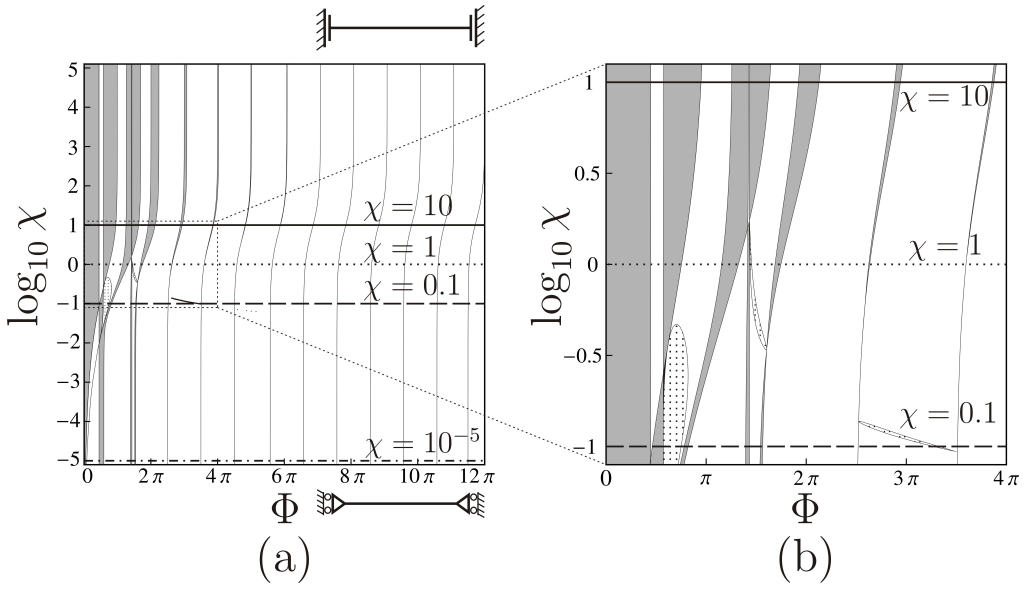

Figure 13: (a) Propagation regions in the physical plane Φ-χ for the periodic beam in Fig. 11; (b) detail of (a). The horizontal lines at $\chi = 0.1, 1, 10$ correspond to the curves in the dispersion diagram in Fig. 12.

to as J_{mp} and m_p, respectively, while the stiffnesses of the corresponding springs are indicated by k_{1p} and k_{2p}.

The transfer matrix for the discrete system of resonators is determined imposing continuity of the kinematic quantities at the junction points, namely continuity of the vector $\boldsymbol{W}$ in the partition (20), while bending moment and shear force jumps at the junction points are obtained from linear and angular momentum balance in the discrete system. The transfer matrix of the discrete phase has the form $\boldsymbol{I} + \boldsymbol{K_p}$, where

$$\boldsymbol{K_p} = \begin{bmatrix} 0 & 0 & 0 & 0 \\ 0 & 0 & 0 & 0 \\ 0 & \frac{k_{1p} J_{mp} \omega^2}{k_{1p} - J_{mp}\omega^2} & 0 & 0 \\ \frac{-k_{2p} m_p \omega^2}{k_{2p} - m_p \omega^2} & 0 & 0 & 0 \end{bmatrix} . \tag{31}$$

Accordingly, the transfer matrix for the unit cell is expressed by

$$\boldsymbol{M}^{[IV]} = \boldsymbol{M}\ (\boldsymbol{I} + \boldsymbol{K_p}) , \tag{32}$$

in which $\boldsymbol{M}$ is again given by Eq. (A.6).

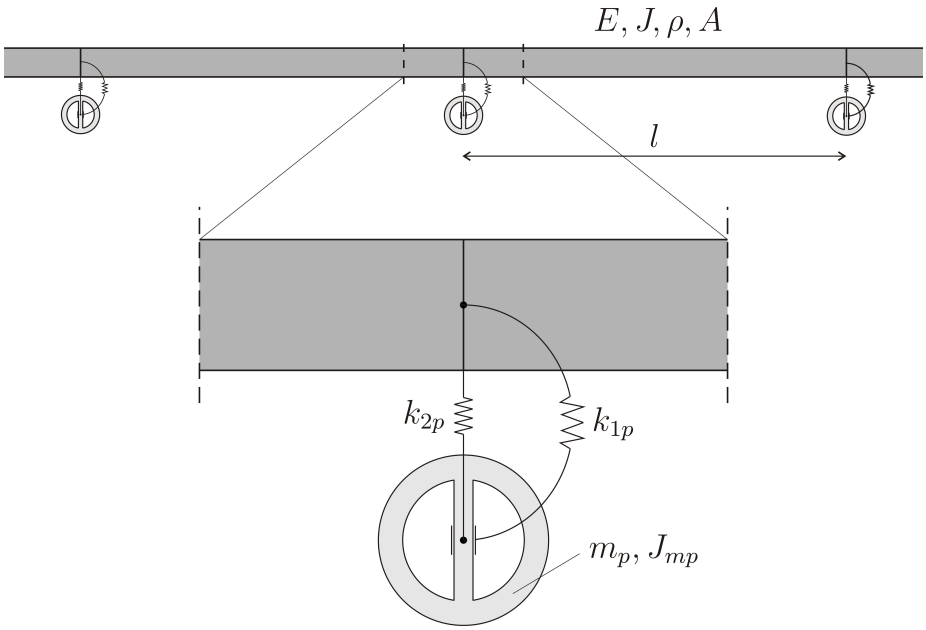

Figure 14: Periodic beam with discrete rotational and translational masses connected in parallel to continuous beam elements.

Similarly to Section 3.3, we define the non-dimensional *frequency parameter*, *inertial ratios* and *stiffness ratios* as

$$\Phi = \beta\, l = \sqrt[4]{\frac{\rho A \omega^2}{EJ}}\, l, \tag{33a}$$

$$M_p = \frac{J_{mp}}{\rho A l^3}, \quad \mu_p = \frac{m_p}{\rho A l}, \tag{33b}$$

$$\kappa_{1p} = \frac{k_{1p} l}{EJ}, \quad \kappa_{2p} = \frac{k_{2p} l^3}{EJ}. \tag{33c}$$

We recall that the natural frequencies of the discrete resonators are

$$\omega_{rot} = \sqrt{\frac{k_{1p}}{J_{mp}}}, \quad \omega_{tr} = \sqrt{\frac{k_{2p}}{m_p}}. \tag{34}$$

The invariants of $\boldsymbol{M}^{[IV]}$ are expressed in terms of the above parameters

as

$$
\begin{aligned}
I_1^{[IV]} =& 2\left[\cos(\Phi)+\cosh(\Phi)\right] - \frac{\Phi}{2}\left[\frac{\kappa_{2p}\mu_p}{\kappa_{2p}-\mu_p\Phi^4}+\frac{\varphi^2\kappa_{2p}M_p\Phi^2}{\varphi^2\kappa_{2p}-\mu_p\Phi^4}\right]\sin(\Phi) \\
&+ \frac{\Phi}{2}\left[\frac{\kappa_{2p}\mu_p}{\kappa_{2p}-\mu_p\Phi^4}-\frac{\varphi^2\kappa_{2p}M_p\Phi^2}{\varphi^2\kappa_{2p}-\mu_p\Phi^4}\right]\sinh(\Phi),
\end{aligned}
\tag{35a}
$$

$$
\begin{aligned}
I_2^{[IV]} =& 2\left[1+2\cos(\Phi)\cosh(\Phi)\right] \\
&+ \frac{\kappa_{2p}^2\Phi}{\left(\kappa_{2p}-\mu_p\Phi^4\right)\left(\varphi^2\kappa_{2p}-\mu_p\Phi^4\right)}\left\{\frac{M_p\mu_p\varphi^2\Phi^3}{2}\left[1-\cos(\Phi)\cosh(\Phi)\right]\right. \\
&- \left[\varphi^2\left(\mu_p+M_p\Phi^2\right)-\frac{\mu_p\Phi^4}{\kappa_{2p}}\left(\mu_p+\varphi^2M_p\Phi^2\right)\right]\cosh(\Phi)\sin(\Phi) \\
&\left.+ \left[\varphi^2\left(\mu_p-M_p\Phi^2\right)-\frac{\mu_p\Phi^4}{\kappa_{2p}}\left(\mu_p-\varphi^2M_p\Phi^2\right)\right]\cos(\Phi)\sinh(\Phi)\right\},
\end{aligned}
\tag{35b}
$$

where $\varphi = \omega_{rot}/\omega_{tr}$ is the *natural frequency ratio*. The invariants $I_1^{[IV]}$ and $I_2^{[IV]}$ are the sum of two distinct contributions: the first due to the continuous phase, with the same expression as in Eq. (17), and the rest due to the presence of the resonators and having singularities at $\Phi = \Phi_{tr} := (\kappa_{2p}/\mu_p)^{1/4}$ and $\Phi = \Phi_{rot} := (\varphi^2\kappa_{2p}/\mu_p)^{1/4}$, corresponding to $\omega = \omega_{tr}$ and $\omega = \omega_{rot}$ respectively.

Dispersion curves are given in Fig. 15a, while propagation zones are shown in the physical plane $\Phi - \varphi$ in Fig. 15b. Results are given for $M_p = \mu_p = 0.01$ and $\kappa_{2p} = 0.25$. The dispersion curves are shown for $\varphi = 0.1, 1, 10$ and for the homogeneous beam case corresponding to $M_p = \mu_p = 0$ or $\kappa_{1p} = \kappa_{2p} = 0$.

Two drastically different behaviors can be obtained depending on the ratio ω_{rot}/ω_{tr}. When $\omega_{rot}/\omega_{tr} < 1$, i.e. $\varphi < 1$, the periodic system behaves as a homogeneous beam at any frequency, except at the rotational ($\Phi = \Phi_{rot}$) and translational ($\Phi = \Phi_{tr}$) natural frequencies of the resonators, where internal resonance modes are excited and extremely narrow stop-bands open up. Narrow stop-bands arise also at $\Phi \sim n\pi$ (n integer) for $kl = 0$ and $kl = \pi$, as shown in the inset of Fig. 15a for $\varphi = 0.1$ and $kl = \pi$. We remind that the presence of stop-bands is associated with stationary modes at the boundaries of the bands. On the contrary, if $\omega_{rot}/\omega_{tr} > 1$ large stop-bands are generated. As $\varphi \to \infty$ the width of stop bands tends to a constant value.

It is important to check the effect of internal resonance modes on the propagation properties of the structured mechanical system. In the case

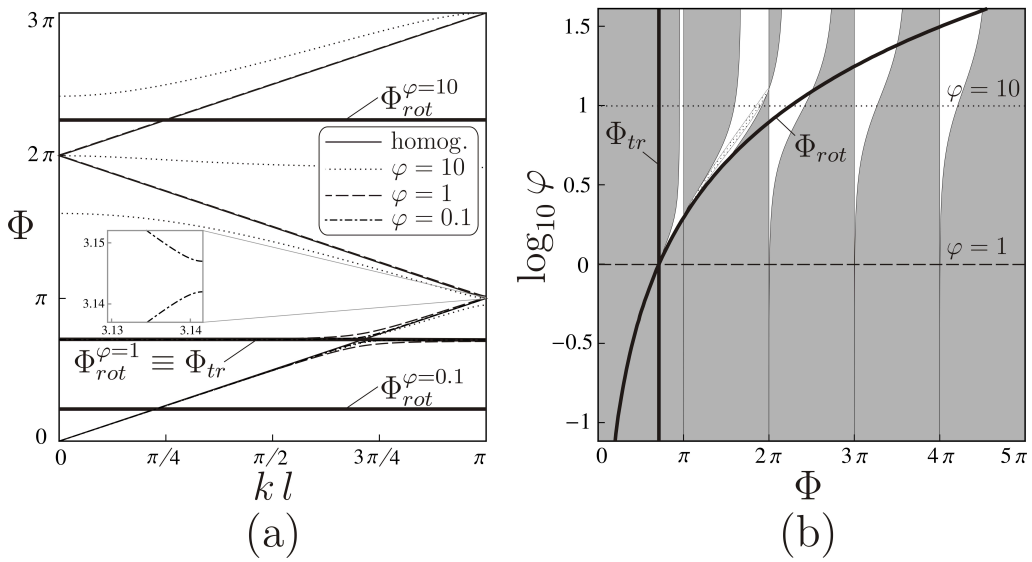

Figure 15: Dispersion curves (a) and physical plane representation of the propagation zones (b) for the periodic beam depicted in Fig. 14 (assuming $M_p = \mu_p = 0.01$ and $\kappa_{2p} = 0.25$).

of continuous beams disposed in parallel analyzed in Section 3.2, resonance modes did not affect the propagation region, while in mono-coupled systems such modes change the propagation type (Brun and Sulis (in preparation)). Here, narrow stop-bands are created in pass-stop regions, while SS regions are not changed in the neighborhood of the internal resonance frequencies. Such conclusion is drawn from the study of the asymptotic behavior of the invariants at the singularities.

The different behavior depending on the ratio ω_{rot}/ω_{tr} is very important in terms of damping of mechanical vibrations. Tuned mass dampers (Den Hartog (1985)) are resonating systems that are often considered as a feasible technology. They are designed to be attached to a structure in order to reduce its dynamic response. The main drawback of this technology is the narrow range of frequency where damping is effective. The results presented in this section show how to extend to a finite frequency range the effect of reduction of vibration amplitude in a mechanical system by simply coupling translation and rotational resonators such that $\omega_{rot} > \omega_{tr}$.

4. Conclusions

This paper has described the propagation of flexural waves in bi-coupled periodic systems, made of unit cells consisting of a continuous beam connected in series or in parallel to another continuous beam or to discrete elements. Propagation and non-propagation regimes have been identified by means of different representations based on the construction of the transfer matrix and imposing quasi-periodic Bloch-Floquet conditions. These representations are dispersion diagram, invariant space, physical space and matrix eigenvalues. The symplectic nature of the transfer matrix allows for great simplifications and direct analytical computations.

Interestingly, systems where two different flexural waves can propagate in both directions have been shown to exist in ranges of frequencies identified as pass-pass regions.

The design of a new generation of tuned mass dampers that can work in a broader range of frequency has been suggested by the introduction of rotational and translational systems of discrete resonators.

The theoretical study performed in this paper may have significant consequences in practical engineering applications, such as for structural health monitoring and imaging. Indeed, the capability of generating bands of non-propagation can be exploited to design mechanical apparatus that control vibrations and reduce noise, and filtering systems that could prevent the transmission of seismic waves or be capable to confine energy propagation within well-identified parts of the structure. To this purpose, we emphasize the considerable usefulness of the representation in the physical space, which allows to easily tune the physical properties of the structure in order to master wave propagation according to the specific design demands.

Acknowledgments

The authors acknowledge the financial support of Regione Autonoma della Sardegna (LR7 2010, grant 'M4' CRP-27585).

References

Wei, J., Petyt, M., 1997a. A method of analyzing finite periodic structures, Part 1: Theory and examples. Journal of Sound and Vibration 202, 555-569.

Wei, J., Petyt, M., 1997b. A method of analyzing finite periodic structures, Part 2: Comparison with infinite periodic structure theory. Journal of Sound and Vibration 202, 571-583.

Brun, M., Giaccu, G.F., Movchan, A.B., Movchan, N.V., 2011. Asymptotics of eigenfrequencies in the dynamic response of elongated multi-structures. Proceedings of the Royal Society A 468, 378-394.

Carta, G., Brun, M., Movchan, A.B., 2014a. Dynamic response and localisation in strongly damaged waveguides. Proceedings of the Royal Society A 470, 20140136.

Carta, G., Brun, M., Movchan, A.B., 2014b. Elastic wave propagation and stop-band generation in strongly damaged solids. Fracture and Structural Integrity 29, 28-36.

Brillouin, L., 1953. Wave propagation in periodic structures: Electric filters and crystal lattices. Dover, New York.

Stroh, A.N., 1962. Steady state problems in anisotropic elasticity. Journal of Mathematical Physics 41, 77-103.

Lekhnitskii, S.G, 1963. Theory of elasticity of an anisotropic elastic body. Holden-Day, San Francisco.

Ting, T.C.T, 1996. Anisotropic elasticity: theory and applications. Oxford University Press, Oxford.

Mead, D.J., 1975a. Wave propagation and natural modes in periodic systems: I. Mono-coupled systems. Journal of Sound and Vibration 40, 1-18.

Mead, D.J., 1975b. Wave propagation and natural modes in periodic systems: II. Multi-coupled systems, with and without damping. Journal of Sound and Vibration 40, 19-39.

Faulkner, M.G., Hong, D.P., 1985. Free vibrations of a mono-coupled periodic system. Journal of Sound and Vibration 99, 29-42.

Martinsson, P.G., Movchan, A.B., 2002. Vibrations of lattice structures and phononic band gaps. Quarterly Journal of Mechanics and Applied Mathematics 56, 45-64.

Brun, M., Guenneau, S., Movchan, A.B., Bigoni, D., 2010. Dynamics of structural interfaces: Filtering and focussing effects for elastic waves. Journal of the Mechanics and Physics of Solids 58, 1212-1224.

Carta, G., Brun, M., 2012. A dispersive homogenization model based on lattice approximation for the prediction of wave motion in laminates. Journal of Applied Mechanics 79, 021019.

Mead, D.J., 1996. Wave propagation in continuous periodic structures: Research contributions from Southampton, 1964-1995. Journal of Sound and Vibration 190, 495-524.

Heckl, M.A., 2002. Coupled waves on a periodically supported Timoshenko beam. Journal of Sound and Vibration 252, 849-882.

Romeo, F., Luongo, A., 2002. Invariants representation of propagation properties for bi-coupled periodic structures. Journal of Sound and Vibration 257, 869-886.

Movchan, A.B., Slepyan, L.I., 2007. Band gap Green's functions and localized oscillations. Proceedings of the Royal Society A 463, 2709-2727.

Movchan, A.B., Slepyan, L.I., 2014. Resonant waves in elastic structured media: Dynamic homogenisation versus Green's functions. International Journal of Solids and Structures 51, 2254-2260.

Movchan, A.B., Movchan, N.V., McPhedran, R.C., 2007. Bloch-Floquet bending waves in perforated thin plates. Proceedings of the Royal Society A 463, 2505-2518.

McPhedran, R.C., Movchan, A.B., Movchan, N.V., 2009. Platonic crystals: Bloch bands, neutrality and defects. Mechanics of Materials 41, 356-363.

Bigoni, D., Movchan, A.B., 2002. Statics and dynamics of structural interfaces in elasticity. International Journal of Solids and Structures 39, 4843-4865.

Gei, M., Movchan, A.B., Bigoni D., 2009. Band-gap shift and defect-induced annihilation in prestressed elastic structures. Journal of Applied Physics 105, 063507.

Brun, M., Movchan, A.B., Slepyan, L.I., 2013. Transition wave in a supported heavy beam. Journal of the Mechanics and Physics of Solids 61, 2067-2085.

Pestel, E.C., Leckie, F.A., 1963. Matrix methods in elastomechanics. McGraw-Hill Inc., New York.

Lekner, J., 1994. Light in periodically stratified media. Journal of the Optical Society of America A 11, 2892-2899.

Castanier, M., Pierre, C., 1995. Lyapunov exponents and localization phenomena in multicoupled nearly periodic systems. Journal of Sound and Vibration 183, 493515.

Brun, M., Movchan, A.B., Jones, I.S., 2013a. Phononic band gap systems in structural mechanics: Finite slender elastic structures and infinite periodic waveguides. Journal of Vibration and Acoustics 135, 041013.

Brun, M., Movchan, A.B., Jones, I.S., McPhedran, R.C., 2013b. Bypassing shake, rattle and roll. Physics World 26, 32-36.

Zuo, L., Nayfeh, S.A., 2005. Optimization of the individual stiffness and damping parameters in multiple-tuned-mass-damper systems. Journal of Vibration and Acoustics 127, 77-83.

Brillouin, L., 1960. Wave propagation and group velocity. Academic Press, New York and London.

Yao, W., Zhong, W., Lim, C.W., 2009. Symplectic Elasticity. World Scientific Publishing Company, Singapore.

Graff, K.F., 1975. Wave motion in elastic solids. Dover Publications Inc., New York.

Carta, G., 2012. Effects of compressive load and support damping on the propagation of flexural waves in beams resting on elastic foundation. Archive of Applied Mechanics 82, 1219-1232.

Brun, M., Sulis, S.. Filtering and focussing effects of elastic waves for different configurations of structural interfaces. *Manuscript in preparation.*

Den Hartog, J.P., 1985. Mechanical Vibrations. Dover Publications Inc., New York.

AppendixA. Transfer matrix of an Euler-Bernoulli beam

The equation of motion of a homogeneous Euler-Bernoulli beam in absence of external loads is

$$EJV^{IV} + \rho A\ddot{V} = 0, \tag{A.1}$$

where EJ is the flexural stiffness, ρA is the mass per unit length and $V = V(x,t)$ represents vertical displacement. Here, roman numbers denote derivatives with respect to the axial coordinate x, while dots indicate derivatives with respect to time t. We consider harmonic waves of the form $V(x,t) = v(x)\exp(\mathrm{i}\omega t)$, with ω denoting the angular frequency. Accordingly, Eq. (A.1) becomes

$$v^{IV} - \beta^4 v = 0, \text{ with } \beta = \sqrt[4]{\frac{\rho A\omega^2}{EJ}}. \tag{A.2}$$

The solution of Eq. (A.2) is given by

$$v(x) = A_1\mathrm{e}^{\beta x} + A_2\mathrm{e}^{-\beta x} + A_3\mathrm{e}^{\mathrm{i}\beta x} + A_4\mathrm{e}^{-\mathrm{i}\beta x}. \tag{A.3}$$

The vector of generalized displacements and forces at the left end of the beam, located at $x = x_l$, can be expressed as

$$\begin{aligned}\boldsymbol{U}(x_l) &= \left\{\begin{array}{c} v(x_l) \\ v'(x_l) \\ -EJv''(x_l) \\ -EJv'''(x_l) \end{array}\right\} = \boldsymbol{S}(x_l)\ \boldsymbol{A} \\ &= \begin{bmatrix} \mathrm{e}^{\beta x_l} & \mathrm{e}^{-\beta x_l} & \mathrm{e}^{\mathrm{i}\beta x_l} & \mathrm{e}^{-\mathrm{i}\beta x_l} \\ \beta\mathrm{e}^{\beta x_l} & -\beta\mathrm{e}^{-\beta x_l} & \mathrm{i}\beta\mathrm{e}^{\mathrm{i}\beta x_l} & -\mathrm{i}\beta\mathrm{e}^{-\mathrm{i}\beta x_l} \\ -EJ\beta^2\mathrm{e}^{\beta x_l} & -EJ\beta^2\mathrm{e}^{-\beta x_l} & EJ\beta^2\mathrm{e}^{\mathrm{i}\beta x_l} & EJ\beta^2\mathrm{e}^{-\mathrm{i}\beta x_l} \\ -EJ\beta^3\mathrm{e}^{\beta x_l} & EJ\beta^3\mathrm{e}^{-\beta x_l} & \mathrm{i}EJ\beta^3\mathrm{e}^{\mathrm{i}\beta x_l} & -\mathrm{i}EJ\beta^3\mathrm{e}^{-\mathrm{i}\beta x_l} \end{bmatrix} \left\{\begin{array}{c} A_1 \\ A_2 \\ A_3 \\ A_4 \end{array}\right\}. \end{aligned} \tag{A.4}$$

By using the equation above, the vector of generalized displacements and forces at the right end of the beam, situated at $x = x_r$, results to be

$$\boldsymbol{U}(x_r) = \left\{\begin{array}{c} v(x_r) \\ v'(x_r) \\ -EJv''(x_r) \\ -EJv'''(x_r) \end{array}\right\} = \boldsymbol{S}(x_r)\ \boldsymbol{A} = \boldsymbol{S}(x_r)\ \boldsymbol{S}^{-1}(x_l)\ \boldsymbol{U}(x_l), \tag{A.5}$$

where $\boldsymbol{S}(x_r)$ is obtained by substituting x_r in place of x_l into Eq. (A.4). The expression of the transfer matrix $\boldsymbol{M}$ can be easily derived from Eq. (A.5):

$$\boldsymbol{M} = \boldsymbol{S}\left(x_r\right)\, \boldsymbol{S}^{-1}\left(x_l\right) = \\ = \begin{bmatrix} \frac{\cos(\beta l)+\cosh(\beta l)}{2} & \frac{\sin(\beta l)+\sinh(\beta l)}{2\beta} & \frac{\cos(\beta l)-\cosh(\beta l)}{2\beta^2 EJ} & \frac{\sin(\beta l)-\sinh(\beta l)}{2\beta^3 EJ} \\ \frac{\beta[-\sin(\beta l)+\sinh(\beta l)]}{2} & \frac{\cos(\beta l)+\cosh(\beta l)}{2} & -\frac{\sin(\beta l)+\sinh(\beta l)}{2\beta EJ} & \frac{\cos(\beta l)-\cosh(\beta l)}{2\beta^2 EJ} \\ \frac{\beta^2 EJ[\cos(\beta l)-\cosh(\beta l)]}{2} & \frac{\beta EJ[\sin(\beta l)-\sinh(\beta l)]}{2} & \frac{\cos(\beta l)+\cosh(\beta l)}{2} & \frac{\sin(\beta l)+\sinh(\beta l)}{2\beta} \\ \frac{-\beta^3 EJ[\sin(\beta l)+\sinh(\beta l)]}{2} & \frac{\beta^2 EJ[\cos(\beta l)-\cosh(\beta l)]}{2} & \frac{\beta[-\sin(\beta l)+\sinh(\beta l)]}{2} & \frac{\cos(\beta l)+\cosh(\beta l)}{2} \end{bmatrix}, \tag{A.6}$$

where $l = x_r - x_l$ is the length of the beam.